Fish and Shellfish Immunology 89 (2019) 437–447

Contents lists available at ScienceDirect

Fish and Shellfish Immunology

journal homepage: www.elsevier.com/locate/fsi

Full length article

A Kunitz proteinase inhibitor (HcKuPI) participated in antimicrobial process during pearl sac formation and induced the overgrowth of calcium carbonate in *Hyriopsis cumingii*

Can Jin[a], Xiao-Jun Liu[a,b,**], Jia-Le Li[a,c,*]

[a] Key Laboratory of Freshwater Aquatic Genetic Resources, Ministry of Agriculture, Shanghai, 201306, China
[b] National Demonstration Center for Experimental Fisheries Science Education, Shanghai Ocean University, Shanghai, 201306, China
[c] Shanghai Engineering Research Center of Aquaculture, Shanghai, 201306, China

ARTICLE INFO

Keywords:
Biomineralization
Matrix protein
Proteinase inhibitors
HcKuPI
Hyriopsis cumingii

ABSTRACT

Proteinase inhibitors with the ability to inhibit specific proteinases are usually closely connected with the immune system. Interestingly, proteinase inhibitors are also a common ingredient in the organic matrix of mollusk shells. However, the molecular mechanism that underlies the role of proteinase inhibitors in immune system and shell mineralization is poorly known. In this study, a Kunitz serine proteinase inhibitor (HcKuPI) was isolated from the mussel *Hyriopsis cumingii*. HcKuPI was specifically expressed in dorsal epithelial cells of the mantle pallium and HcKuPI dsRNA injection caused an irregular surface and disordered deposition on the aragonite tablets of the nacreous layer. These results indicated that HcKuPI plays a vital role in shell nacreous layer biomineralization. Moreover, the expression pattern of HcKuPI during LPS challenge and pearl formation indicated its involvement in the antimicrobial process during pearl sac formation and nacre tablets accumulation during pearl formation. In the *in vitro* calcium carbonate crystallization assay, the addition of GST-HcKuPI increased the precipitation rate of calcium carbonate and induced the crystal overgrowth of calcium carbonate. Taken together, these results indicate that HcKuPI is involved in antimicrobial process during pearl formation, and participates in calcium carbonate deposition acceleration and morphological regulation of the crystals during nacreous layer formation. These findings extend our knowledge of the role of proteinase inhibitors in immune system and shell biomineralization.

1. Introduction

Biomineralization is the process by which organic macromolecules interact with inorganic ions at an interface and the biomacromolecules regulate and control the crystallization of inorganic minerals, thereby allowing the mineral to undergo an elaborate assembly process and develop special hierarchical structures. The mollusk shell is a typical biomineral, and it provides protection for the visceral mass. In general, the longitudinal section of shell contains the combination of highly insoluble periostracum, prismatic layer, and nacreous layer [1,2]. In the calcified layer, calcium carbonate is the major element, whereas biomacromolecules such as polysaccharides, matrix proteins, lipids, and polypeptide account for only about 5% (w/w) [3]. Despite this low proportion, biomacromolecules, especially matrix proteins, play a dominant role in determining crystal nucleation and morphology, which provide excellent mechanical properties for shells [4,5].

Numerous studies in recent years have shown that biomineralization system of mollusks is closely associated with its immune system. It is common sense that hemocytes are essential for innate immuse responses [6], previous studies also documented that hemocyte is an absolutely necessary component for biomineralization process, such as grafting and shell regeneration [7]. Hemocytes always accumulate in the gaps between mantle graft and host tissues during pearl sac formation, and the residual haemocytes within the nucleus cavity could induce low-quality pearl formation [8]. Besides, haemocytes in extrapallial fluid also have the capacity to induce $CaCO_3$ nucleate and further transfer them to the mineralization front during shell regeneration [9,10].

Proteinase inhibitors with the ability to inhibit specific proteinases are usually closely connected with the immune system. While, proteinase inhibitors are also ubiquitous ingredient in the shell organic matrix. For example, proteinase inhibitors were found in the water-soluble

* Corresponding author. Key Laboratory of Freshwater Aquatic Genetic Resources, Ministry of Agriculture, Shanghai, 201306, China.
** Corresponding author. Key Laboratory of Freshwater Aquatic Genetic Resources, Ministry of Agriculture, Shanghai, 201306, China.
E-mail addresses: txliuxj@vip.163.com (X.-J. Liu), jlli2009@126.com (J.-L. Li).

https://doi.org/10.1016/j.fsi.2019.04.021
Received 28 January 2019; Received in revised form 6 March 2019; Accepted 7 April 2019
Available online 11 April 2019
1050-4648/

shell matrix of the oyster *Pinctada margaritifera*, and nacre organic proteinases showed activity against several serine proteinases in a subsequent proteinase inhibition assay [11]. In the mantle transcriptome of the mussel *Mytilus edulis* and the oyster *Pinctada maxima*, several potential peptide fragment contained a Kunitz-like type II domain [12,13]. Subsequently, proteomic analysis revealed the presence of proteinase inhibitor domains in the shell matrix of different mollusk species [14–20]. However, the molecular mechanism that regulates how proteinase inhibitors function in immune and shell mineralization systems is poorly known because only tiny amounts of related protein have been isolated.

Among the known matrix proteins, lustrin A, which is a nacre protein of the abalone *Haliotis rufescens*, shares homology with a mammalian serine proteinase inhibitor, but a functional study has not been performed [21]. MSP22.8 of the mussel *Mytilus galloprovincialis*, which is a serpin-like protein, was found to be expressed in the shell organic matrix, mantle edge, extrapallial fluid (EPF), and EP hemocytes [22]. Furthermore, MSP22.8 had two biological effects: it was transported by EP hemocytes to the shell as part of the matrix framework, and it prevented proteolytic damage to other constituents of the organic matrix to help the biomineralization process run smoothly [22,23]. The existence of proteinase inhibitors in the mollusk shell is also thought to be involved in immunological defense [24], promoting matrix maturation [25], and inhibiting crystal formation [26].

Despite evidence that proteinase inhibitors are common in the mollusk shell matrix, few protease inhibitors have been isolated and their main roles in immune and shell mineralization systems are poorly explored. In this study, the matrix protein HcKuPI (Kunitz-type serine protease inhibitor), was isolated from the mussel *H. cumingii*. After tissue-specific gene expression analysis, the expression pattern during pearl formation was analyzed, and the nacreous layer was observed by scanning electron microscopy (SEM) as part of an RNA interference (RNAi) assay. Additionally, the recombinant protein glutathione S-transferase (GST)-HcKuPI was successfully expressed and purified to validate the direct connection between the protease inhibitor and calcium carbonate crystals using *in vitro* calcium carbonate crystallization experiments.

2. Materials and methods

2.1. RNA extraction

H. cumingii (length about 7–8 cm, about 2-years-old) used in the experiment were purchased from the Wuyi Pearl Farm in Jinhua, China. Adductor muscle (AM), foot (F), mantle (M), gill (GI), hepatopancreas (H), blood (B), and gonad (G) tissue samples were collected separately. After grinding the tissue in liquid nitrogen, total RNA was extracted using TRIzol reagent (Life Technologies, Carlsbad, CA, USA) according to the manufacturer's instructions. For each tissue, after quality and concentration detection, equal amounts of RNA (totally 1 μg) were mixed and synthesized to cDNA using the SMART RACE cDNA Amplification kit (Clontech Bio. Inc., Dalian, China) for rapid amplification of cDNA ends (RACE). Total RNA of each tissue (500 ng) then was reverse-transcribed to cDNA following the instructions of the PrimeScript™ RT reagent kit (Takara Bio. Inc., Dalian, China) for tissue-specific gene expression analysis.

2.2. RACE and bioinformatics analysis

According to the amino acid sequence “GGCGGN” of the matrix protein papilin in the oyster *Crassostrea gigas*, a degenerate primer was designed for 3′ RACE polymerase chain reaction (PCR) (Table 1). After amplification using the Advantage 2 cDNA polymerase mix, the products were further analyzed by sequencing. A specific primer then was used for 5′ RACE PCR based on the result of 3′ RACE (Table 1). After sequencing, the products of 3′ RACE and 5′RACE was spliced. The following programs then were used to analyze the results: The open reading frame (ORF) was detected by ORF Finder (http://www.ncbi.nlm.nih.gov/projects/gorf/); protein domain prediction was performed by SMART (http://smart.embl-heidelberg.de/); homology analysis was performed by GenBank and BLAST; the signal peptide was analyzed by the SignalIP4.1 Server (http://www.cbs.dtu.dk/services/SignalP/); the amino acid sequence of the mature protein was analyzed by ExPasy (http://web.expasy.org/protparam/); putative phosphorylation sites were detected by the NetPhos 2.0 server (http://www.cbs.dtu.dk/services/NetPhos/); glycosylation sites prediction was performed by the YinOYang 1.2server (http://www.cbs.dtu.dk/services/YinOYang/); and protein structure prediction was performed by Phyre2 (http://www.sbg.bio.ic.ac.uk/phyre2/html/page.cgi?id=index).

2.3. Tissue-specific gene expression analysis

Based on the complete nucleotide sequence of HcKuPI, a pair of gene-specific primers was designed for reverse transcription PCR (RT-PCR) and quantitative real-time PCR (qRT-PCR), and EF-1α was used as the internal reference (Table 1). RT-PCR was carried out in a 20 μL reaction system containing 10 μL of 2 × Taq master mix (Novoprotein Scientific, Inc., Jiangsu, China), 0.8 μL of each primer (10 mM), 2 μL of cDNA (60 ng/μL), and 6.4 μL of RNase-free water. The cycling parameters for RT-PCR were as follows: 94 °C initial denaturation for 3 min (one cycle), 94 °C denaturation for 5s, 58 °C annealing for 30s, 72 °C extension for 30s (40 cycles), and 72 °C for 10 min (one cycle). The PCR products then were detected by agarose gel electrophoresis. The reaction system and program for qRT-PCR were similar to those for RT-PCR. SYBR qPCR super mix (Novoprotein Scientific) was used for the amplification reaction. Based on the crossing-point (CT) values, the relative expression of HcKuPI in different tissues was calculated using equation $2^{-\Delta\Delta Ct}$, (ΔCT = CT of the target – CT of EF-1α, ΔΔCT = ΔCT of the challenged sample – ΔCT of the calibration sample). Data from the qRT-PCR experiments were expressed as the means ± standard error (SE).

2.4. In situ hybridization

A specific segment of HcKuPI was amplified by specific primers (Table 1), and the anti-sense probe of HcKuPI was synthesized using the T7 high-efficiency transcription kit (TransGen Biotech, Beijing, China) according to manufacturer's instructions with some modification. Briefly, T7 transcription was carried out for 2 h at 37 °C in a 10 μL reaction system containing 4 μL of purified PCR product (200 ng), 2 μL of 5 × T7 Transcription Reaction Buffer, 2 μL of DIG RNA Labeling Mix (Roche Diagnostics, Basel, Switzerland), and 2 μL of T7 Transcription Enzyme Mix. The anti-sense probe was hybridized with a 10 μm mantle tissue slice overnight (about 20 h), and after hybridization with Anti-digoxigenin-AP Conjugate and NBT/BCIP colouration (Roche Diagnostics), the hybridization signals were photographed.

2.5. Temporal expression of HcKuPI after LPS challenge

Total 80 adult *H. cumingii* were used in LPS challenge assay, and 40 mussels were challenged with LPS as experimental group, 40 mussels were challenged with PBS as control group. Blood and mantle of five mussels were collected at 0, 3, 6, 12, 24, 36, 48 and 96 h after challenge. After RNA extraction and cDNA synthesis, qRT-PCR and data handling was performed as described above, and HcKuPI transcript in blood at 0 h time point was performed as calibration sample.

2.6. Pearl culture assay

A pearl culture assay was conducted to detect the expression pattern of HcKuPI during pearl formation. Two hundred *H. cumingii* were used in the pearl cultivation experiment. Epithelial cells from the mantle

Table 1
Primers used in experiments.

Primer	Sequence (5' - 3′)	Usage
HcKuPI-F	GGNGGNTGYGGNGGNAAY (N = A/G/C/T; Y=C/T)	RACE
HcKuPI-R	GGCAGTCTTTCCTCCACATCGTT	RACE
HcKuPI-RT/qRT-PCR-F	ACGGTCAGGGAAGAAGAAAAAAGGA	RT/qRT-PCR
HcKuPI-RT/qRT-PCR-R	ACAGGCGCTACGCGAAGTAAAGTTA	RT/qRT-PCR
EF-1a-F	GGAACTTCCCAGGCAGACTGTGC	RT/qRT-PCR
EF-1a-R	TCAAAACGGGCCGCAGAGAAT	RT/qRT-PCR
HcKuPI-ISH−F	CCGTCATCAGAAGGACAAAGTAACA	ISH
HcKuPI-ISH-R + T7	GGATCCTAATACGACTCACTATAGGCGGTACAGATCGGTTTCATTGTACT	ISH
HcKuPI-RNAi-F	CCGTCATCAGAAGGACAAAGTAACA	RNAi
HcKuPI-RNAi-F + T7	GGATCCTAATACGACTCACTATAGGCCGTCATCAGAAGGACAAAGTAAC	RNAi
HcKuPI-RNAi-R	CGGTACAGATCGGTTTCATTGTACT	RNAi
HcKuPI-RNAi-R + T7	GGATCCTAATACGACTCACTATAGGCGGTACAGATCGGTTTCATTGTACT	RNAi
GFP-RNAi-F	AAGGGCGAGGAGCTGTTCACCG	RNAi
GFP-RNAi-F + T7	GGATCCTAATACGACTCACTATAGGAAGGGCGAGGAGCTGTTCACCG	RNAi
GFP-RNAi-R	CAGCAGGACCATGTGATCGCGC	RNAi
GFP-RNAi-R + T7	GGATCCTAATACGACTCACTATAGGCAGCAGGACCATGTGATCGCGC	RNAi
HcKuPI-YH−F	CGGAATTCCAACGGTCAGGGAAGAAGAAAAAAG	Prokaryotic expression
HcKuPI-YH-R	TTTTCCTTTTGCGGCCGCTTAGGCAGTCTTTCCTCCACATCGT	Prokaryotic expression

edge of 100 individuals were made into small strips (saibos) (0.5 cm × 0.5 cm) and transplanted into the center of the mantle of the other 100 individuals. On days 3, 5, 8, 11, 15, 18, and 25, six mussels were collected and the pearl sacs were stored in RNAStore (Tiangen, Beijing, China). After RNA extraction, the RNA was synthesized into cDNA. The qRT-PCR reaction was conducted and relative expression of HcKuPI during pearl formation was analyzed as described above. One-way analysis of variance was perfomed by SPSS18.0 to determine whether there are any significant differences, and significance was accepted at the level of $p < 0.05$.

2.7. RNA-mediated interference (RNAi) assays of HcKuPI during nacreous layer formation

The RNAi assays was performed as described by Pan et al. [27] with some modifications. Briefly, double stranded (ds) RNA synthesis was performed using the T7 RiboMAX™ Express RNAi system according to the manufacturer's instructions (Promega, Madison, WI, USA). The dsRNA was diluted to concentrations of 20 μg/100 μL and 40 μg/100 μL using phosphate buffered saline (PBS) and injected into the adductor muscle of five mussels. HcKuPI dsRNA was the experimental group, and green fluorescent protein (GFP) dsRNA and PBS injection served as the negative and blank groups, respectively. At day 7 after injection, treated individuals were collected and shells were cut into sections. The internal surface of each shell was observed under a SEM. The mantle tissue also was harvested, RNA was extracted, cDNA was synthesized, and qPT-PCR was performed as described above. Furthermore, significance comparison was performed by SPSS 18.0, and significance was accepted at the level of $p < 0.01$.

2.8. Expression and purification of recombinant GST-HcKuPI protein

The full-length of HcKuPI (with signal peptide sequences removed) was amplified using the specific primers HcKuPI-EcoRI-F (containing EcoR I restriction site) and HcKuPI-Not I-R (containing Not I restriction site). After double enzyme restriction, the purified PCR product was subcloned into the prokaryotic expression vector pGEX-4T-1, and the reading frame was confirmed to be correct by sequencing. The recombinant plasmid pGEX-4T-1/HcKuPI was transformed into Rosetta (DE3) competent cells. The host strain first was cultured at 37 °C to $OD_{600} = 0.6$, and then isopropyl-β-d-thiogalactoside (IPTG) was added to a final concentration of 2 mM for the inducible expression of recombinant protein.

After induction for 10 h at 18 °C, the bacterial cells were harvested by centrifuging (10,000 rpm, 20 min), and the thalli were resuspended with bacteria lysate and sonicated on ice. The supernatant was collected after centrifugation at 10,000 rpm for 20 min, and inclusion body protein was dissolved in 8 M urea solution. After filtration using a membrane syringe filter (0.22 μm), protein purification was performed according to the specifications of the GST prepacked column (Novoprotein Scientific). The eluant component was concentrated and purified by ultrafiltration (10 kDa cutoff, Millipore, Burlington, MA, USA), then the recombinant protein was dissolved in Milli-Q water and analyzed by 12% polyacrylamide gel electrophoresis.

2.9. In vitro calcium carbonate crystallization assay

A saturated calcium bicarbonate solution was prepared as described by Xu et al. [28] with some modification. First, 1.2 g of calcium carbonate power (purity > 99.9%) were mixed with 100 mL of Milli-Q water, then the solution was ventilated with carbon dioxide and stirred continuously overnight. The supernatant then was collected and filtered using a syringe filter (0.22 μm). The recombinant protein GST-HcKuPI was mixed with saturated calcium bicarbonate solution on siliconized glass as the experimental group. Saturated calcium bicarbonate solution mixed with bovine serum albumin (BSA) or GST served as the control groups. After storing for 48 h in a sealed box, the siliconized glass was analyzed using a Renishaw RM2000 Raman spectroscopy device (Bruker, Ettlingen, Germany) to evaluate crystal polymorphism, and SEM was used to examine crystal morphology.

2.10. In vitro calcium carbonate precipitation rate assay

The effect of HcKuPI on the precipitation rate of calcium carbonate was evaluated following the experimental method Suzuki et al. [29] with some modification. Briefly, in the experimental group, 10 μL of recombinant protein GST-HcKuPI solution were mixed with 100 μL of 20 mM $NaHCO_3$ (pH 8.5) in a 96-well Elisa plate, and then 100 μL of 20 mM $CaCl_2$ were added to each well. In the control groups, 10 μL of Milli-Q water or GST protein solution were mixed with the $NaHCO_3$ and $CaCl_2$ as the blank group. The sedimentation rate of the mixture was recorded once per min for a total of 5 min by reading the absorbance at 570 nm on SpectraMax190 (Molecular Devices Corporation, CA, USA).

3. Results

3.1. Isolation and bioinformatics analysis of HcKuPI

Using RACE, a 621 base pair (bp) transcript was amplified from mantle tissue cDNA. The transcript contained a 333 bp ORF coding 110

A

```
1                                                                   GTGAGAGAAACCGTCATCAGAAGGACAAAGTAACAACTTTTCTAAGTTGACGGCGCTGGAA
62    ATG  CAG  TGG  AAA  AGA  CAT  TTT  CTC  GTC  TTC  GTA  CTG  ATA  ATT  GCA  CTG  TTC  GTC  AGC  AAC
1     M    Q    W    K    R    H    F    L    V    F    V    L    I    I    A    L    F    V    S    N
122   TTT  GTG  GAA  GCA  CAA  CGG  TCA  GGG  AAG  AAG  AAA  AAA  GGA  AAA  AGT  AAA  TCT  AAA  GAT  GTG
21    F    V    E    A    Q    R    S    G    K    K    K    K    G    K    S    K    S    K    D    V
182   ATT  AGT  TCT  TTA  ACA  CTC  CCA  GAA  AAT  GAT  CAG  CAA  GAT  GTA  TGC  AAA  CAA  CCG  AAA  GAA
41    I    S    S    L    T    L    P    E    N    D    Q    Q    D    V    C    K    Q    P    K    E
242   GTA  GGA  CCA  TGC  AAA  GGG  AAG  ATA  AAG  AGA  TAT  TAC  TTC  AAG  AAG  GAA  TCA  GGA  AAA  TGC
61    V    G    P    C    K    G    K    I    K    R    Y    Y    F    K    K    E    S    G    K    C
302   AAA  TCA  TTT  AAT  TTT  GGC  GGC  TGT  GGG  GGC  AAC  GAA  AAT  AAC  TTT  ACT  TCG  CGT  AGC  GCC
81    K    S    F    N    F    G    G    C    G    G    N    E    N    N    F    T    S    R    S    A
362   TGT  CGA  AAA  CGA  TGT  GGA  GGA  AAG  ACT  GCC  TAA  AATGATTTCACCTCTCAAAACCAGTGTCCAGGATTCTTTAGACACCT
101   C    R    K    R    C    G    G    K    T    A    *
442   AAAAAAATGAAAAAAAAATGAAAAAAGTACAATGAAACCGATCTGTACCGGACCACAGTTTACGTTCTTGCTCTGCGCATAACAGAACGCTGTTTAGAGCTGCAA
547   GTATCAAGCATTAAGAAGAATGGTCTGTTGAATTGTGATTAAAGCGTACAGACATAAAAAAAAAAAAAAAAAAAAA
```

B

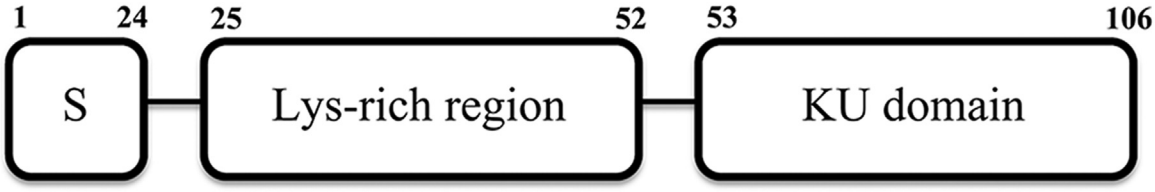

C

D

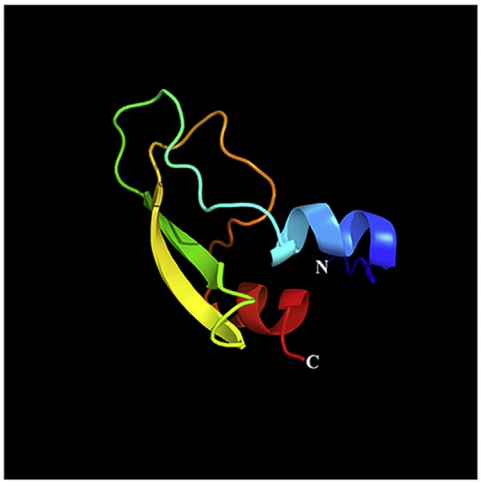

E

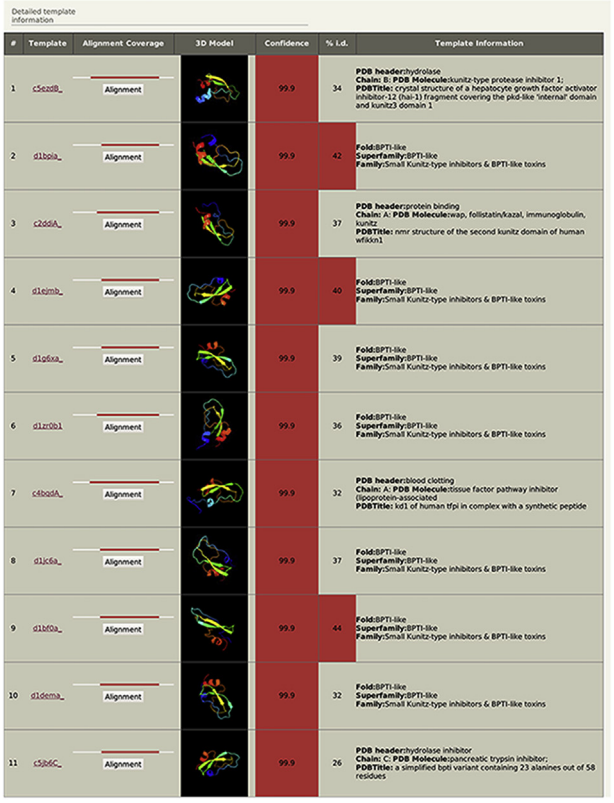

(caption on next page)

Fig. 1. Bioinformatics analysis of HcKuPI. A, The full-length cDNA and putative amino acid sequence of HcKuPI. The initiation codon (ATG) and termination codon (TAA) are marked by imaginary line. The putative signal peptide is underlined. The putative O-glycosylation sites are marked by wavy line, and putative phosphorylation sites are boxed. B, The modular structure of HcKuPI. S, signal peptide. C, Based on the protein sequence of HcKuPI, the secondary structure prediction is performed by Phyre[2]. The amino acids are colored based on the physiochemical properties of the side chains. The regions adopting putative α-helix and β-sheet conformations are represented as green spiral and blue arrow, respectively. The degrees of confidence 0.9 are also indicated by a rainbow color gradient. D, The tertiary structure of HcKuPI performed by Phyre[2]. E, Detailed information about template in the secondary structure prediction. (For interpretation of the references to color in this figure legend, the reader is referred to the Web version of this article.)

Table 2
The amino acid content and composition of the mature protein.

Amino acid	Percent %	Amino acid	Percent %
Lys	20.9%	Asp	3.5%
Gly	12.8%	Pro	3.5%
Ser	10.5%	Thr	3.5%
Cys	7.0%	Val	3.5%
Arg	5.8%	Ala	2.3%
Asn	5.8%	Ile	2.3%
Gln	4.7%	Leu	2.3%
Glu	4.7%	Tyr	2.3%
Phe	4.7%		
*M*w [kDa]	9.5kD	*p*I	9.96

amino acids (Fig. 1 A). The bioinformatics analysis showed that the deduced protein contained a Kunitz domain and that it shared high homology with other Kunitz-type inhibitors (based on BLASTP retrieval) (Fig. 1 E). Therefore, the mature protein was referred to as HcKuPI, an abbreviation for Kunitz-type serine protease inhibitor from *Hyriopsis cumingii*. Furthermore, the first 24 amino acids in the N-terminal constituted a signal peptide that caused HcKuPI to be secreted into the extracellular space (Fig. 1A). The molecular weight of the mature protein was 9.5 kD, and the amino acid composition of mature protein HcKuPI was characterized by high proportions of lysine (20.9%), glycine (12.8%), and serine (10.5%). Its theoretical isoelectric point was 9.96 (Table 2). Posttranslational modification prediction revealed two glycosylation sites (^{27}S and ^{109}T) and four potential phosphorylation sites on Ser (position 27, 35, 37, and 77) (Fig. 1 A). Overall, the amino acid sequence of HcKuPI exhibited a remarkable modular structure, including the N-terminal signal peptide (residues 1–24), the lysine-rich region (residues 25–52), and the C-terminal Kunitz domain (residues 53–106) (Fig. 1 B). The cDNA sequence of HcKuPI was submitted to Genbank under accession no. MH796550. The structure prediction showed that the secondary structure of HcKuPI is composed of α-helices (21%) and β-strands (21%) (Fig. 1 C). The potential tertiary structure of HcKuPI was characterized by a distorted antiparallel β-sheet and a regular α-helix section in the C-terminal (Fig. 1 D).

3.2. Expression analysis of HcKuPI

Relative expression of HcKuPI in different tissues was first detected by RT-PCR. Agrose gel electrophoresis analysis showed that the HcKuPI gene was expressed specifically in the mantle, and it was not detectable in any other tissues (Fig. 2 A). qRT-PCR detection showed that HcKuPI was expressed mainly in the mantle, but a negligible amount was found in the adductor muscle, no expression was detected in the foot, gill, hepatopancreas, blood and gonad (Fig. 2 B). Due to different functions of each region within mantle tissue, we further analyzed the location of HcKuPI in the mantle by *in situ* hybridization. In experimental group, the hybridization signals were mainly detected in dorsal epithelial cells of the mantle pallium, and no signals were detected in epithelial cells of the periostracal groove and mantle edge. While, no signal in the dorsal epithelial cells of the mantle pallium was detected in negative control group (Fig. 2 C).

3.3. Relative expression of HcKuPI after LPS challenge

After LPS challenge, qRT-PCR was performed to determine the expression pattern of HcKuPI in mantle and blood. As shown in Fig. 3, the expression of HcKuPI in mantle did not significantly increase before 36 h after LPS challenge, but peaked at 48 h and returned to normal level at 96 h. Compared with mantle tissue, the levels of HcKuPI transcript in blood were very low. HcKuPI was significantly increased in the blood at 6 h, and almost no expression at other time points.

3.4. Relative expression of HcKuPI during pearl calcification

In the pearl graft transplantation experiment, pearl sacs were harvested to detect the expression pattern of HcKuPI during pearl formation. Relatively high expression of HcKuPI was first detected on days 3 and 5 after implantation, then it decreased and returned to normal levels on day 8. In subsequent days, the expression of HcKuPI increased, peaking on day 18 and remaining high on day 25 (Fig. 4).

3.5. Effects of HcKuPI during shell nacreous layer formation

To further explore the role of HcKuPI in nacre formation, HcKuPI dsRNA was injected into the adductor muscle in the experimental group. The relative mRNA level of HcKuPI in the experimental group exhibited a significant and sustained decline as the concentration of HcKuPI dsRNA increased (Fig. 5 A). Compared with PBS and GFP treated groups, the expression level of HcKuPI decreased to 60% in the 20 μg injected group and to about 50% in the 40 μg injected group (Fig. 5 A).

SEM observation of the microstructure of the nacreous-layer surface in the GFP and PBS injected groups showed that the newborn tablet had a regular shape and a distinct boundary (Fig. 5 B, C). In the experimental group, the newborn crystals exhibited an obscure boundary, irregular surface and disordered deposition (Fig. 5 D, E).

3.6. Expression and purification of the recombinant HcKuPI protein

The full-length mature protein HcKuPI gene (except for the signal peptide) was cloned by PCR and further subcloned into the pGEX-4T-1 vector after double enzyme restriction. The bacteria solution PCR conducted using primers pGEX5′ and pGEX3′ revealed a band of about 430 bp in the recombinant plasmid pGEX-4T-1/HcKuPI and a band of about 170 bp in the vector pGEX-4T-1, which indicated that the recombinant plasmid was constructed successfully (Fig. 6 A). The recombinant plasmid pGEX-4T-1/HcKuPI was transformed into Rosetta (DE3) competent cells and induced by IPTG (2 mM) for 10 h at 18 °C. The supernatant of the lysate was purified using a GST prepacked column and analyzed by SDS-PAGE. The recombinant protein of GST-HcKuPI was present mainly in the supernatant of the bacteria lysate: a visible band (recombinant protein GST-HcKuPI) of about 34 kDa was detected in the experimental group, and a visible band (protein GST) of about 25 kDa was detected in the control group (Fig. 6 B).

3.7. Calcium carbonate precipitation and crystallization assay

The recombinant protein GST-HcKuPI was mixed with saturated calcium carbonate solution, and absorbance was recorded at 570 nm to

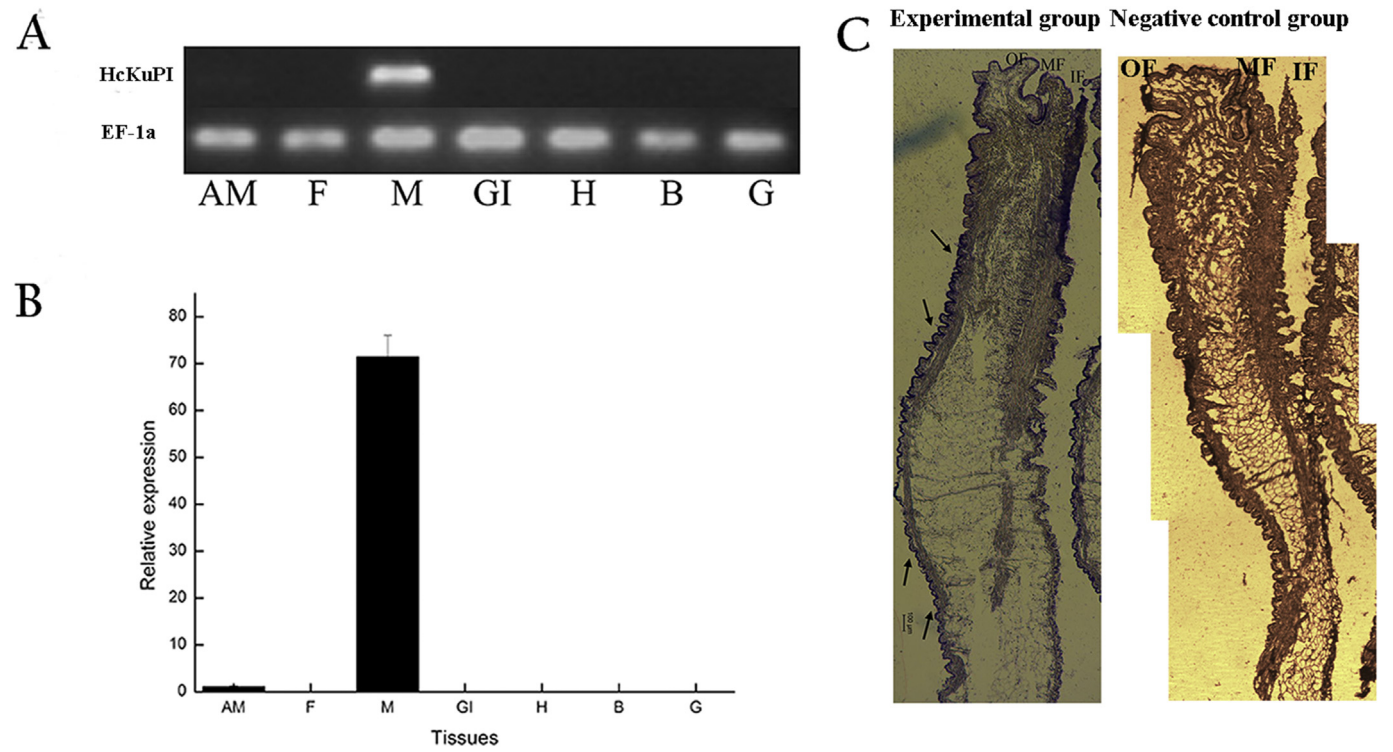

Fig. 2. Gene expression pattern of HcKuPI. A, tissue-specific gene expression of HcKuPI by RT-PCR. B, tissue-specific gene expression of HcKuPI by qRT-PCR. AM, adductor muscle; F, foot; M, mantle; GI, gill; H, hepatopancreas; B, blood; G, gonad. C, *In situ* hybridization analysis of *HcKuPI* expression in the *Hyriopsis cumingii* mantle. IF, inner fold; MF, middle fold; OF, outer fold.

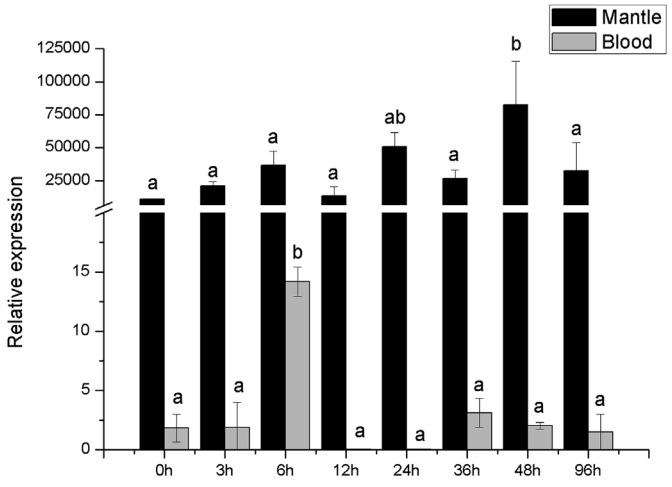

Fig. 3. Relative expression of HcKuPI in mantle and blood after LPS challenge.

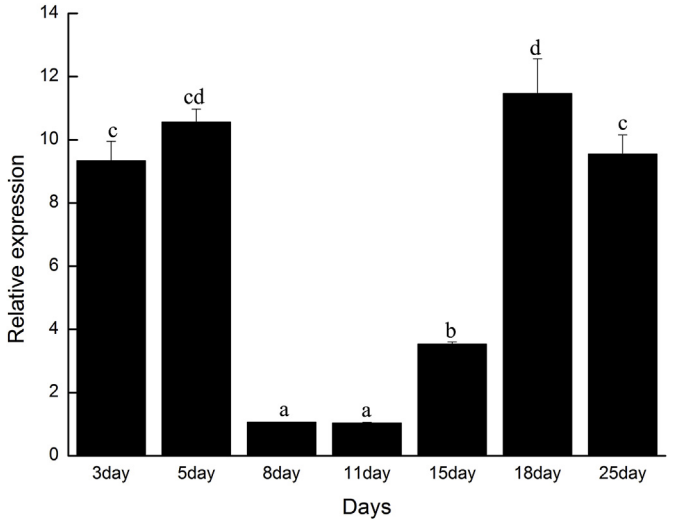

Fig. 4. Relative expression of HcKuPI in the pearl sac during the early stages of pearl formation after implantation.

determine the sedimentation rate of calcium carbonate. The precipitation rate of the GST added group was similar to that of the Milli-Q water added group. The precipitation rate of the GST-HcKuPI group was significantly higher than that of the control group (Milli-Q water/GST addition), and the precipitation rate increased with increasing GST-HcKuPI concentration (Fig. 7).

In the *in vitro* crystallization assay, GST-HcKuPI in a concentration gradient was mixed with saturated calcium carbonate solution. In the control group (BSA/GST addition), the microstructure of the deposited crystal was characterized by typical rhombohedra with a smooth surface (Fig. 8 M, N, P, and Q). In the low dose GST-HcKuPI group (10 μg/mL), additional quadrate granule deposition on the rhombohedra surface occurred, and the surface of this additional deposition was smooth (Fig. 8A–C). However, the presence of a higher dose of GST-HcKuPI (20 μg/mL) resulted in a rough surface on some of the deposited crystal, and this roughness consisted mainly of club-shaped granule (Fig. 8D–F). In the high dose GST-HcKuPI group (40 μg/mL), the crystal was roughly circular and its surface was consisted of a number of cylindrical aragonite fibers, these aragonite fibers congregated in clumps and vertically grow on the top surface (Fig. 8G–I). Furthermore, the microstructure of deposition in the 50 μg/mL GST-HcKuPI group also consisted of cylindrical aragonite fibers, and further detection showed the cylindrical aragonite fibers were consisted of the subgrains, which was vertical growth and arranged in an orderly fashion (Fig. 8J–L). Raman analysis showed that the surface of the crystals in both the control and experimental groups had the distinct Raman spectra of calcite (Fig. 8 O and R).

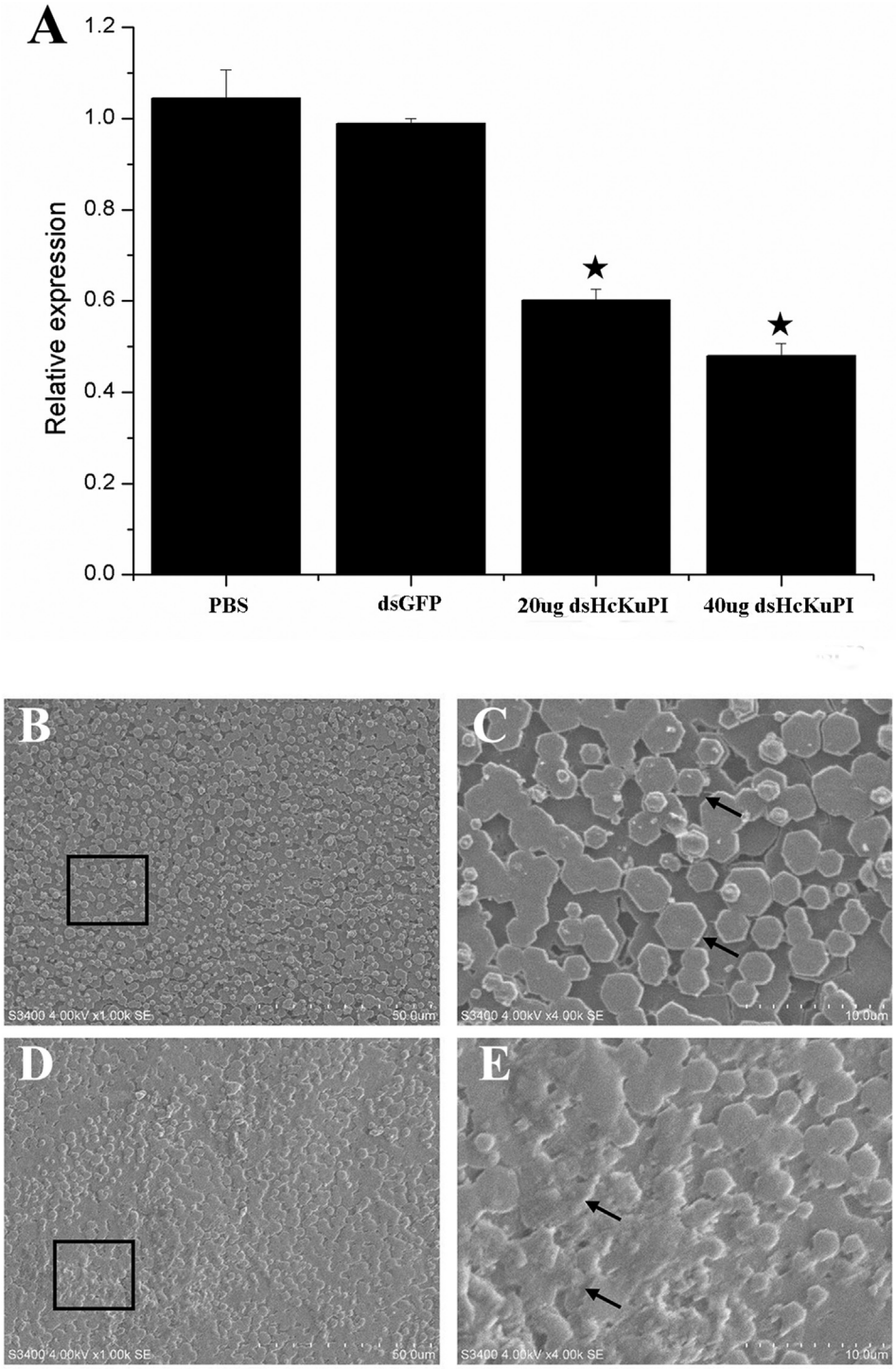

Fig. 5. Effects of HcKuPI knockdown by RNAi. A, Attenuated *HcKuPI* expression after RNAi. For the control, expression levels in the PBS-injected group were measured to a relative value of 1.0. *p < 0.01 compared with the PBS-injected group. B and C, SEM image of the inner surface of normal shells, the normal tablets are boxed and enlarged in C. D and E, SEM image of the inner surface of experimental group, the irregular tablets are boxed and enlarged in E.

4. Discussion

Serine proteinase inhibitors with strong ability to inhibit specific proteinases are closely connected to the immune system. In vertebrates, they specifically affect serine protease and are involved in the anti-inflammatory process [30]. In invertebrates, serine proteinase inhibitors are generally play a role in many physiological and pathological processes, including fighting microbial infection and blood clotting [31–33]. Therefore, previous studies of serine protease inhibitors in aquatic animals focused mainly on their antimicrobial activity in the immune response [31,34,35]. In this study, we isolated a novel matrix protein gene, HcKuPI, from *H. cumingii*. The mature HcKuPI peptide contained a Kunitz motif and shares 40–60% homology with other Kunitz-type inhibitors, which suggested that HcKuPI was a Kunitz-type protease inhibitor.

Generally, serine proteinase inhibitors first combine with hemocytes before they play an important role in immune system. While, gene expression analysis showed that HcKuPI was highly expressed in the

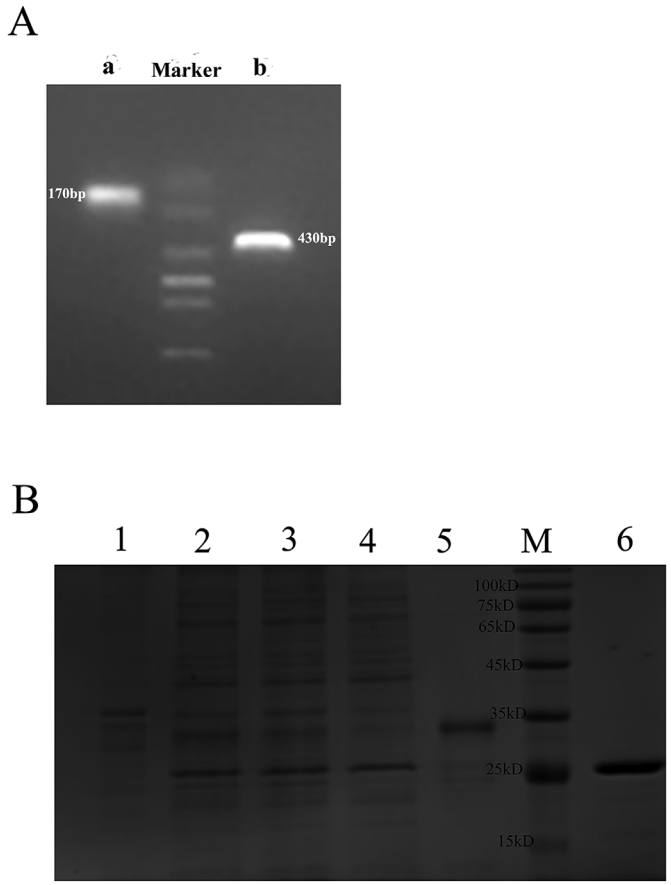

Fig. 6. Expression and purification of recombinant protein GST-HcKuPI. A, agarose gel electrophoresis analysis of recombinant plasmid. B, the expression and purification of recombinant HcKuPI protein, 1, inclusion-body protein. 2–3, flow-through. 4, impurity protein. 5, eluent of recombinant protein. 6, marker. 7, eluent of GST protein.

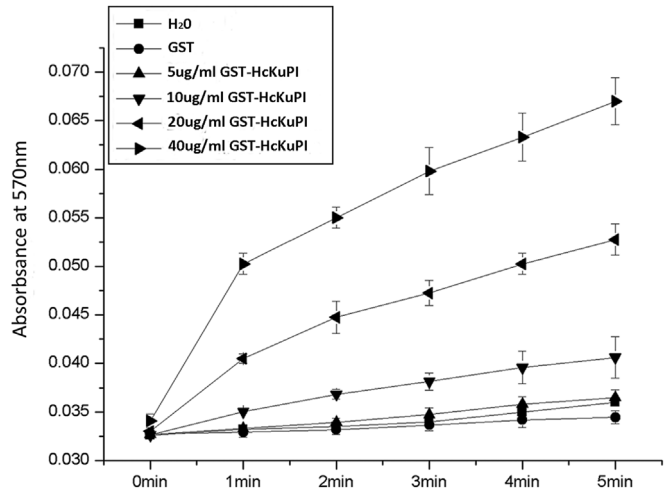

Fig. 7. Effects of HcKuPI on calcium carbonate precipitation., H_2O was used as a negative control; ●, GST;, 5 μg/mL GST-HcKuPI;, 10 μg/mL GST-HcKuPI;, 20 μg/mL GST-HcKuPI;, 40 μg/mL GST-HcKuPI.

mantle, and almost not detectable in hepatopancreas present in the circulatory system, and the expression of HcKuPI in mantle increased significantly at 48 h after LPS challenge. A previous study showed that KuSPI of *H. cumingii* is also not expressed in hepatopancreas, and the expression of KuSPI was even the highest in mantle after *Aeromonas hydrophila* infection [35]. Therefore, HcKuPI could be involved in inhibiting environmental microbes. Moreover, the levels of HcKuPI transcript in blood was significant high at 6 h after LPS challenge, and almost no detectable at other time points, indicating its involvement in antimicrobial process. The hypothesis was verified in this study using the pearl culture assay. Previous studies have demonstrated that graft operation could cause pathogen invasion, massive hemocytes always accumulate in the gaps between mantle graft and host tissues [8], and immune related genes always respond to pearl sac formation. The high expression of HcKuPI was first appeared at day 3 and 5 during pearl sac formation, and low expression was appeared after pearl sac formation. These results indicated HcKuPI might combine with the hemocytes secreted by mantle and further involve in the antimicrobial process during pearl sac formation.

In shellfish, the mantle is a vital tissue that is responsible for secreting matrix proteins to regulate shell formation, and specific areas of the mantle are in charge of processing different calcified layers biomineralization [36]. Briefly, the outer epithelium of the edge in the outer fold accounts for prismatic layer formation, and the dorsal region participates in nacreous layer formation. HcKuPI was highly expressed in the dorsal epithelial cells of the mantle pallium. Therefore, HcKuPI might be a matrix protein that is mainly involved in nacreous layer calcification. Moreover, the mRNA level of HcKuPI in the pearl sac was significantly high between days 18 and 25. During pearl formation, a disordered prismatic layer first is deposited on the nucleus and then an ordered nacreous layer forms on the organic membrane [37]. In a previous study, tawny pearls of *H. cumingii* were first collected on day 14 after implantation, and pearls with fine luster were harvested on day 21 [38]. Furthermore, the decreased expression of HcKuPI in RNAi induced abnormal morphology of the shell in the nacreous layer. All results indicated that HcKuPI was essential for nacreous layer formation.

The bioinformatics analysis showed that the amino acid sequence of HcKuPI shared typical features with other matrix proteins, which exhibited a remarkable modular structure and mainly were composed of several specific amino acids. A putative signal peptide was located in the N-terminal region, which mainly accounted for protein secretion, and a lysine-rich basic region was located in the central region. In some known matrix proteins, the basic region is thought to interact effectively with anionic molecules such as CO_3^{2-} and HCO_3^{-} [39]; it also may be involved in intermolecular cross-linking via Schiff's base conjugates [40]. The basic part could also interact with acidic soluble proteins. An acidic region (ENDQQD, residues 48–53) was also found in the lysine-rich basic region, and it mainly interacted with Ca^{2+} to participate in crystal formation [41]. Additionally, a KU domain was located in the C-terminal. Kunitz-type serine protease inhibitors usually have a highly conserved tertiary structure. Six Cys residues located in the KU domain promote formation of intramolecular disulfide bonds to maintain its space conformation and biological activity, and the inhibiting effects of the domain are determined by five active sites. Briefly, the P1 residue is the principal determinant of inhibitor specificity, and the P1′ residue affects the association constant values between protease inhibitor and protease [42]. The P1 and P1′ residues of HcKuPI were found to be Lys and Gly, respectively, indicating that HcKuPI mainly inhibited trypsin. Finally, the basic C-terminal region (RKRCGGKTA) may effectively interact with other matrix proteins [43]. Therefore, the role of HcKuPI in shell mineralization likely involves preventing proteolytic damage of other matrix proteins and binding with other functional matrix protein to directly regulate nacreous layer formation.

The pathway by which proteinase inhibitors participate in shell biomineralization has been poorly understood. Because proteinase inhibitors usually are located in plasma and blood and are involved in the immune response, proteinase inhibitors involved in shell formation were thought to be abundant in hemocytes [27]. However, HcKuPI was specifically expressed in the mantle, and it was not detected in hemocytes. Bivalves have an open circulatory system, in addition to the

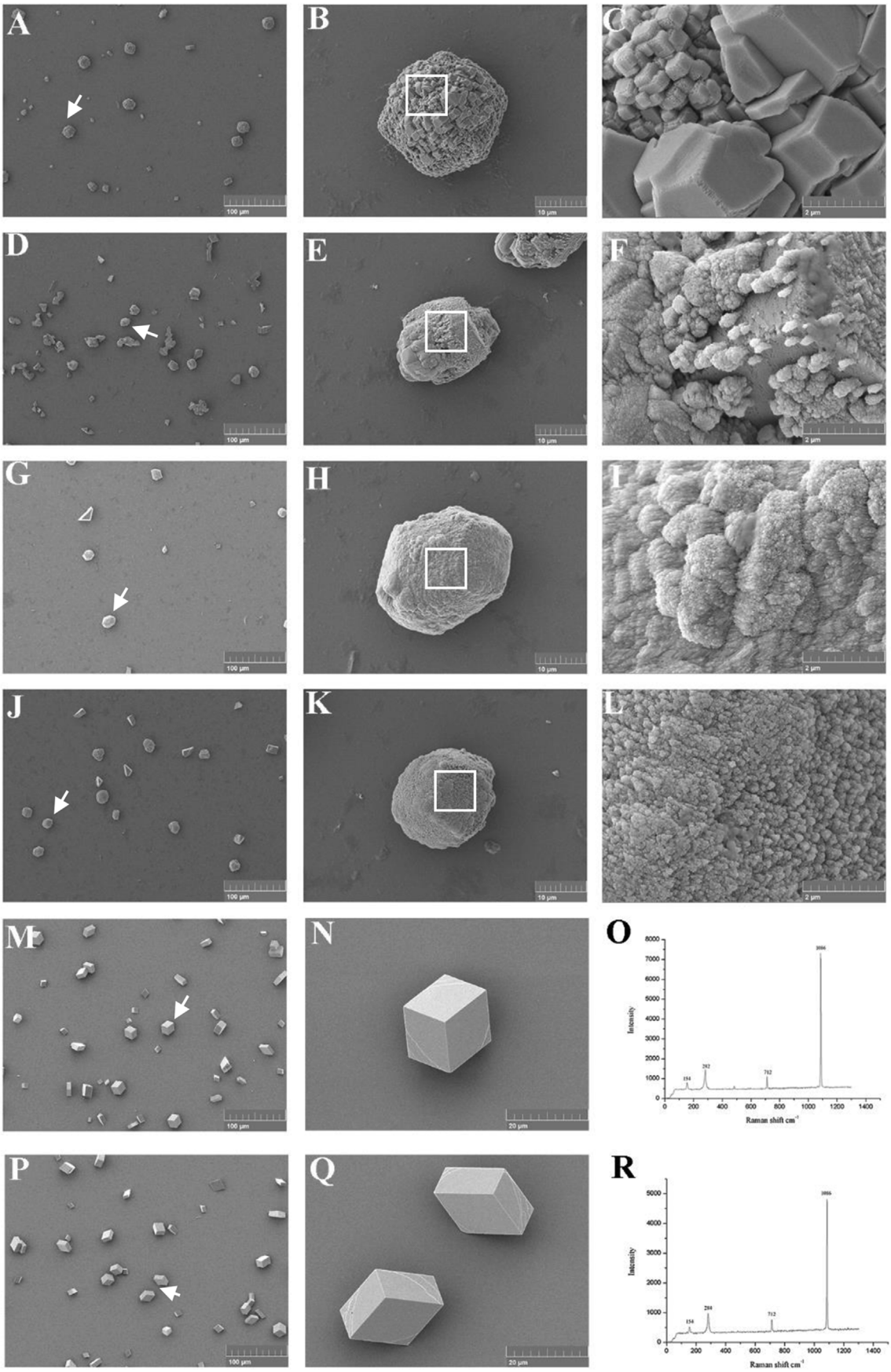

Fig. 8. SEM images of *in vitro* crystallization experiments in the presence of HcKuPI and the resulting Raman spectra. A-C, crystallization in 10 μg/mL HcKuPI group. D-F, crystallization in 20 μg/mL HcKuPI group. G-I, crystallization in 40 μg/mL HcKuPI group. J-L, crystallization in 50 μg/mL HcKuPI group. M and N, crystallization in BSA group. P and Q, crystallization in GST group. O, Raman spectra of the crystals formed in the blank group and R, in the experimental group.

circulatory system, hemocytes are also abundant in mucosal tissues (e.g. gills and digestive tract) [44]. Recently, hemocytes were detectable in mantle tissue and further migration by epithelium [45]. Calvo-Iglesias et al. isolated a protease inhibitor-like protein (MSP22.8) from *M. galloprovincialis* [22], and its monoclonal antibody was not detectable in hemolymph extracted from adductor muscle but it was detectable in hemolymph extracted from EPF [23]. Additionally, numerous studies have illustrated the involvement of hemocytes in the mineralization process (e.g., in shell formation and the regeneration process) [9,10]. During shell regeneration, an increasing number of calcium-bearing granulocytes in EPF are fused into shell sheets and finally translocated to the mature area of regenerated shell [7,46,47]. Therefore, Mount et al. hypothesized that the granulocyte part of hemocytes is secreted by the outer surface of the mantle center, and crystals are translocated to nucleation sites [48]. Therefore, HcKuPI might first be secreted by the mantle pallium into the EPF, followed by transportation by granulocytes to the mineralization front where it can prevent proteolytic damage of other matrix proteins and participate in biomineralization process directly.

To explore the involvement of HcKuPI in crystal regulation, the recombinant protein GST-HcKuPI was expressed and purified. Results of the *in vitro* crystallization assay showed that the addition of GST-HcKuPI increased calcium carbonate precipitation and led to crystal overgrowth. In previous study, after crystal nucleation, the changes of pH and inorganic ion concentrations in extrapallial fluid could further regulated the exposed aragonite crystals overgrow in mature nacre, but it was uncertain that whether the process is strictly controlled by matrix protein [49]. In present study, GST-HcKuPI could induce crystal overgrowth directly and the morphology of the overgrowth crystals was precisely controlled by the dose of GST-HcKuPI. As GST-HcKuPI concentration increased, the overgrowth deposition changed from columnar grains to cylindrical aragonite fibers, and the stacking manner was also changed from disordered accumulation to ordered accumulation. These results indicated HcKuPI could combine with the hemocytes within extrapallial fluid and further involved in deposition acceleration and morphological regulation at a nanometer scale.

In conclusion, HcKuPI might combine with hemocytes in mantle tissue and involve in the antimicrobial process during pearl sac formation. Moreover, HcKuPI can directly interact with calcium carbonate to increase precipitation and morphological regulation during nacreous layer formation. More in-depth studies of HcKuPI will provide more information about the molecular mechanism by which proteinase inhibitors affect shell mineralization.

Conflicts of interest

The authors declare that they have no conflict of interest.

Acknowledgments

This work was financially supported by the National Natural Science Foundation of China (31672654), the Modern Agro-industry Technology Research System (CARS-49), and the Project of Shanghai Engineering and Technology Center for Promoting Ability (16DZ2281200). We also thank International Science Editing (http://www.internationalscienceediting.com) for editing this manuscript.

References

[1] G. Bevelander, H. Nakahara, An electron microscope study of the formation and structure of the periostracum of a gastropod, Littorina littorea, Calcif. Tissue Res. 5 (1) (1970) 1–12.
[2] X. Liu, J. Li, Formation of the prismatic layer in the freshwater bivalve Hyriopsis curninqii: the feedback of crystal growth on organic matrix, Acta Zool. 96 (1) (2015) 30–36.
[3] S. Weiner, W. Traub, S.B. Parker, Macromolecules in mollusc shells and their functions in biomineralization [and discussion], Phil. Trans. Roy. Soc. Lond. 304 (1121) (1984) 425–434.
[4] A.G. Checa, A.B. Rodríguez-Navarro, F.J. Esteban-Delgado, The nature and formation of calcitic columnar prismatic shell layers in pteriomorphian bivalves, Biomaterials 26 (32) (2005) 6404–6414.
[5] A. Lia, J. Derk, N. Fabio, W. Steve, Mollusk shell formation: a source of new concepts for understanding biomineralization processes, Chem. Eur J. 12 (4) (2006) 980–987.
[6] L. Song, L. Wang, H. Zhang, M. Wang, The immune system and its modulation mechanism in scallop, Fish Shellfish Immunol. 46 (1) (2015) 65–78.
[7] S. Li, Y. Liu, C. Liu, J. Huang, G. Zheng, L. Xie, R. Zhang, Hemocytes participate in calcium carbonate crystal formation, transportation and shell regeneration in the pearl oyster Pinctada fucata, Fish Shellfish Immunol. 51 (2016) 263–270.
[8] P. Kishore, P.C. Southgate, A detailed description of pearl-sac development in the black-lip pearl oyster, Pinctada margaritifera (Linnaeus 1758), Aquacult. Res. 47 (7) (2016) 2215–2226.
[9] J. Huang, S. Li, Y. Liu, C. Liu, L. Xie, R. Zhang, Hemocytes in the extrapallial space of Pinctada fucata are involved in immunity and biomineralization, Sci. Rep. 8 (1) (2018).
[10] A.V. Ivanina, H.I. Falfushynska, E. Beniash, H. Piontkivska, I.M. Sokolova, Biomineralization-related specialization of hemocytes and mantle tissues of the Pacific oysters Crassostrea gigas, J. Exp. Biol. 220 (18) (2017) jeb.160861.
[11] L. Bedouet, D. Duplat, A. Marie, L. Dubost, S. Berland, M. Rousseau, C. Milet, E. Lopez, Heterogeneity of proteinase inhibitors in the water-soluble organic matrix from the oyster nacre, Mar. Biotechnol. 9 (4) (2007) 437–449.
[12] A. Freer, S. Bridgett, J. Jiang, M. Cusack, Biomineral proteins from Mytilus edulis mantle tissue transcriptome, Mar. Biotechnol. 16 (1) (2014) 34–45.
[13] D.J. Jackson, C. Mcdougall, B. Woodcroft, P. Moase, R.A. Rose, M. Kube, R. Reinhardt, D.S. Rokhsar, C. Montagnani, C. Joubert, Parallel evolution of nacre building gene sets in molluscs, Mol. Biol. Evol. 27 (3) (2010) 591.
[14] Z. Liao, L.-f. Bao, M.-h. Fan, P. Gao, X.-x. Wang, C.-l. Qin, X.-m. Li, In-depth proteomic analysis of nacre, prism, and myostracum of Mytilus shell, J. Proteom. 122 (2015) 26–40.
[15] B. Marie, J. Arivalagan, L. Matheron, G. Bolbach, S. Berland, A. Marie, F. Marin, Deep conservation of bivalve nacre proteins highlighted by shell matrix proteomics of the Unionoida Elliptio complanata and Villosa lienosa, J. R. Soc. Interface 14 (126) (2017).
[16] B. Marie, A. Marie, D.J. Jackson, L. Dubost, B.M. Degnan, C. Milet, F. Marin, Proteomic analysis of the organic matrix of the abalone Haliotis asinina calcified shell, Proteome Sci. 8 (2010).
[17] B. Marie, I. Zanella-Cléon, R.N. Le, M. Becchi, G. Luquet, F. Marin, Proteomic analysis of the acid-soluble nacre matrix of the bivalve Unio pictorum: detection of novel carbonic anhydrase and putative protease inhibitor proteins, Chembiochem 11 (15) (2010) 2138–2147.
[18] C. Le Pabic, A. Marie, B. Marie, A. Percot, L. Bonnaud-Ponticelli, P.J. Lopez, G. Luquet, First proteomic analyses of the dorsal and ventral parts of the Sepia officinalis cuttlebone, J. Proteom. 150 (2017) 63–73.
[19] C. Liu, S. Li, J. Kong, Y. Liu, T. Wang, L. Xie, R. Zhang, In-depth proteomic analysis of shell matrix proteins of Pinctada fucata, Sci. Rep. 5 (2015).
[20] B. Marie, D.J. Jackson, P. Ramos-Silva, I. Zanella-Cleon, N. Guichard, F. Marin, The shell-forming proteome of Lottia gigantea reveals both deep conservations and lineage-specific novelties, FEBS J. 280 (1) (2013) 214–232.
[21] X. Shen, A.M. Belcher, P.K. Hansma, G.D. Stucky, D.E. Morse, Molecular cloning and characterization of lustrin A, a matrix protein from shell and pearl nacre of Haliotis rufescens, J. Biol. Chem. 272 (51) (1997) 32472–32481.
[22] J. Calvo-Iglesias, D. Perez-Estevez, A. Gonzalez-Fernandez, MSP22.8 is a protease inhibitor-like protein involved in shell mineralization in the edible mussel Mytilus galloprovincialis, Febs Open Bio 7 (10) (2017) 1539–1556.
[23] J. Calvo-Iglesias, D. Pérez-Estévez, S. Lorenzo-Abalde, B. Sánchez-Correa, M.I. Quiroga, J.M. Fuentes, Á. González-Fernández, Characterization of a monoclonal antibody directed against Mytilus spp larvae reveals an antigen involved in shell biomineralization, PLoS One 11 (3) (2016) e0152210.
[24] J. Keith, S. Stockwell, D. Ball, K. Remillard, D. Kaplan, T. Thannhauser, R. Sherwood, Comparative analysis of macromolecules in mollusc shells, Comp. Biochem. Physiol. Part B Comparat. Biochem. 105 (3–4) (1993) 487–496.
[25] C. Dombre, N. Guyot, T. Moreau, P. Monget, M. Da Silva, J.L. Gautron, S. Réhault-Godbert, Egg Serpins: the Chicken And/or the Egg Dilemma, Seminars in Cell & Developmental Biology.
[26] L. Treccani, K. Mann, F. Heinemann, M. Fritz, Perlwapin, an abalone nacre protein with three four-disulfide core (whey acidic protein) domains, inhibits the growth of calcium carbonate crystals, Biophys. J. 91 (7) (2006) 2601.
[27] C. Pan, D. Fang, G. Xu, J. Liang, G. Zhang, H. Wang, L. Xie, R. Zhang, A novel acidic matrix protein, PfN44, stabilizes magnesium calcite to inhibit the crystallization of aragonite, J. Biol. Chem. 289 (5) (2014) 2776–2787.
[28] G.F. Xu, N. Yao, I.A. Aksay, J.T. Groves, Biomimetic synthesis of macroscopic-scale calcium carbonate thin films. Evidence for a multistep assembly process, J. Am. Chem. Soc. 120 (46) (1998) 11977–11985.
[29] S. Michio, M. Emi, I. Hirotaka, O. Noriaki, T. Hidekazu, K. Toshihiro, N. Hiromichi, Characterization of Prismalin-14, a novel matrix protein from the prismatic layer of the Japanese pearl oyster (Pinctada fucata), Biochem. J. 382 (Pt 1) (2004) 205.
[30] H. Shigetomi, A. Onogi, H. Kajiwara, S. Yoshida, N. Furukawa, S. Haruta, Y. Tanase, S. Kanayama, T. Noguchi, Y. Yamada, Anti-inflammatory actions of serine protease inhibitors containing the Kunitz domain, Inflamm. Res. 59 (9) (2010) 679–687.
[31] H.N. Mai, H.T.N. Nguyen, K. Koiwai, H. Kondo, I. Hirono, Characterization of a Kunitz-type protease inhibitor (MjKuPI) reveals the involvement of MjKuPI positive hemocytes in the immune responses of kuruma shrimp Marsupenaeus japonicus, Dev. Comp. Immunol. 63 (2016) 121–127.

[32] M.S. Bajaj, J.J. Birktoft, S.A. Steer, S.P. Bajaj, Structure and biology of tissue factor pathway inhibitor, Thromb. Haemostasis 86 (04) (2001) 959–972.
[33] J. Rojtinnakorn, I. Hirono, T.Y. Itami, T. Aoki, Gene expression in haemocytes of kuruma prawn, Penaeus japonicus, in response to infection with WSSV by EST approach, Fish Shellfish Immunol. 13 (1) (2002) 69–83.
[34] L. Zhu, L. Song, Y. Chang, W. Xu, L. Wu, Molecular cloning, characterization and expression of a novel serine proteinase inhibitor gene in bay scallops (Argopecten irradians, Lamarck 1819), Fish Shellfish Immunol. 20 (3) (2006) 320–331.
[35] Y. Wang, L. Xu, G. Wang, C. Wu, J. Li, Cloning and expression analysis of KuSPI gene of hypriopsis cumingii, Genom. Appl. Biol. 36 (6) (2017) 2374–2379.
[36] T. Takeuchi, K. Endo, Biphasic and dually coordinated expression of the genes encoding major shell matrix proteins in the pearl oyster Pinctada fucata, Mar. Biotechnol. 8 (1) (2006) 52–61.
[37] X.J. Liu, J.L. Li, L. Xiang, J. Sun, G.L. Zheng, G.Y. Zhang, H.Z. Wang, L.P. Xie, R.Q. Zhang, The role of matrix proteins in the control of nacreous layer deposition during pearl formation, Proc. Biol. Sci. 279 (1730) (2012) 1000–1007.
[38] J.Y. Lin, K.Y. Ma, Z.Y. Bai, J.L. Li, Molecular cloning and characterization of perlucin from the freshwater pearl mussel, Hyriopsis cumingii, Gene 526 (2) (2013) 210–216.
[39] C. Zhang, L.P. Xie, J. Huang, X.L. Liu, R.Q. Zhang, A novel matrix protein family participating in the prismatic layer framework formation of pearl oyster, Pinctada fucata, Biochem. Biophys. Res. Commun. 344 (3) (2006) 735–740.
[40] J. Gordon, M.R. Carriker, Sclerotized protein in the shell matrix of a bivalve mollusc, Mar. Biol. 57 (4) (1980) 251–260.
[41] S. Weiner, L. Hood, Soluble protein of the organic matrix of mollusk shells: a potential template for shell formation, Science 190 (4218) (1975) 987–989.
[42] J. Otlewski, M. Jaskã³Lski, O. Buczek, T. Cierpicki, H. Czapiå„Ska, D. Krowarsch, A.O. Smalas, D. Stachowiak, A. Szpineta, M. Dadlez, Structure-function relationship of serine protease-protein inhibitor interaction, Acta Biochim. Pol. 48 (2) (2001) 419–428.
[43] B.A. Wustman, J.C. Weaver, D.E. Morse, J.S. Evans, Structure-function studies of the Lustrin A polyelectrolyte domains, RKSY and D4, Connect. Tissue Res. 44 (2003) 10–15.
[44] B. Allam, E.P. Espinosa, Bivalve immunity and response to infections: are we looking at the right place? Fish Shellfish Immunol. 53 (2016) 4–12.
[45] Y.-T. Lau, L. Sussman, E.P. Espinosa, S. Katalay, B. Allam, Characterization of hemocytes from different body fluids of the eastern oyster Crassostrea virginica, Fish Shellfish Immunol. 71 (2017) 372–379.
[46] E. Kadar, A. Lobo-Da-Cunha, C. Azevedo, Mantle-to-shell CaCO 3 transfer during shell repair at different hydrostatic pressures in the deep-sea vent mussel Bathymodiolus azoricus (Bivalvia: mytilidae), Mar. Biol. 156 (5) (2009) 959–967.
[47] S.M. Cho, W.G. Jeong, Prismatic shell repairs by hemoctyes in the extrapallial fluid of the Pacific Oyster, Crassostrea gigas, Korean J. Malacol. 27 (3) (2011) 223–228.
[48] A.S. Mount, A.P. Wheeler, R.P. Paradkar, D. Snider, Hemocyte-mediated shell mineralization in the eastern oyster, Science 304 (5668) (2004) 297–300.
[49] R. Giles, S. Manne, S. Mann, D.E. Morse, G.D. Stucky, P.K. Hansma, Inorganic overgrowth of aragonite on Molluscan nacre examined by atomic force microscopy, Biol. Bull. 188 (1) (1995) 8–15.